THREE DIMENSIONAL MODELING OF COMBUSTION PROCESS AND EMISSION FORMATION IN A LOW HEAT REJECTION INDIRECT INJECTION DIESEL ENGINE

by

Samad JAFARMADAR* * and Jalilpour BEHROUZ

Department of Mechanical Engineering, Urmia University, Urmia, Iran

Original scientific paper
DOI: 10.2298/TSCI130203126J

Higher heat losses and brake specific fuel consumption are major problems in an indirect injection diesel engine, which can be overcome by means of low heat rejection concept. This concept is based on the approach of insulating of piston and liner of main chamber in an indirect injection engine. At the present work, the combustion process and emission formation in baseline and low heat rejection engines are studied by a computational fluid dynamics code at four different loads (25%, 50%, 75%, and 100%) in maximum torque engine speed of 730 rpm. The numerical results for the pressure in cylinder and emissions for baseline engine at full load operation are compared to the corresponding experimental data and show good agreement. The comparison of the results for two cases show that when the load increases from 25% to 100% in 25% steps, heat loss in low heat rejection engine decrease 40.3%, 44.7%, 44.6%, and 45.2%, respectively. At full load operation in low heat rejection engine, NO_x and soot emissions decrease 13.5% and 54.4%, respectively, and engine efficiency increases 6.3% in comparison to baseline engine.

Key words: *combustion, emission, indirect injection, low heat rejection, three dimensional modeling, load*

Introduction

The combustion characteristics of the indirect injection (IDI) engines are different from direct injection (DI) engines, because of high turbulence intensity and greater heat-transfer losses in the swirl chamber [1-4]. This defect causes the brake-specific fuel consumption (BSFC) of the IDI engine to increase and the total engine efficiency to decrease compared to that of a DI diesel engine. Because of these disadvantages of the IDI diesel engines, most engine research has focused on the DI diesel engines. However, because of higher air velocity and rapidly occurring air-fuel mixture formation in both combustion chambers of the IDI diesel engines, these engines have a simple fuel injection system and lower injection pressure level [5, 6]. In addition, they do not depend upon the fuel quality and cetane number [5, 6] and produce lower exhaust emissions [7] than DI diesel engines. Especially, unburned hydrocarbon (HC) and carbon monoxide (CO) emissions are significantly lower in these engines, which have homogeny charge condition [8, 9]. Beside thermal efficiency decreases in IDI engine in comparison to DI engine because of higher heat loss from cylinder wall. The concept of low heat rejection (LHR) engine aims to reduce this great heat loss transferred to cooling system in an IDI engine. So, this energy can be converted to useful work [10]. Some of the major advantages of LHR engines in-

* Corresponding author; e-mail: s.jafarmadar@urmia.ac.ir.

clude better fuel economy, increased engine life, reduction in HC, CO and particulate matter (PM) emissions, and lower combustion noise due to reduced pressure increasing rate, increased exhaust gases exergy, and ability operating lower cetane fuels [11-17]. Also, the higher temperatures in the combustion chamber at LHR engine can have a positive effect on diesel engines at adiabatic case, due to the self-ignition delay drop [18].

A lot of experimental study has been done to utilize LHR engines concept to improve thermal efficiency by reducing heat losses, and to improve mechanical efficiency by eliminating cooling systems. The experimental investigations of Parlak *et al*., [19] and Buyukkaya and Cerit [20] revealed that with the proper adjustment of the injection timing, it is possible to partially offset the adverse effect of insulation on heat release rate and hence to obtain improved performance and lower NO_x. Dickey [21] carried out experimental investigations about insolated engines and showed that a decreased ignition delay and premixed fraction and a corresponding and increased in the amount of fuel burned during the diffusion phase of combustion were take place in the case of LHR engine. The experiments of Jaichandar and Tamilporai [22] and Amann [23] have shown that high temperature operation of LHRE cause considerable improvement in fuel consumption and thermal efficiency, an increased in availability in the exhaust gas and NO formation, a reduction of soot formation. According to studying of Wang *et al*. [24], the characteristics of high temperature combustion, the methods, such as decreasing hole diameter, optimizing injection timing, and employing a special type of impingement plate in the combustion chamber which breaks the envelope of high temperature flame, can reduce the combustion duration, achieve high efficiency and low soot emission in LHR engines. Also, experimental investigation on the effect of ceramic coatings on diesel engine performance and exhaust emissions which was performed by Assanis *et al*. [25] shows that in the optimum thickness of ceramic coating, efficiency increases, and emissions decreases. Another experimental investigation about the study of energy balance was carried out by Taymaz [26] in low heat rejection diesel engine. Numerical studies about energy and exergy of exhaust gas stream, which is the most important source of available energy and exergy in a LHRE, have been performed by many different authors [27-29] at the optimum injection timing. Many fundamental aspects concerning of CFD simulation of IDI engines have been discussed earlier by Pinchon [30]. Three dimensional modeling of combustion process and soot formation in an indirect injection diesel engine using KIVA CFD code has been performed by Zellat *et al*. [31]. Strauss and Schweimer [32] studied the combustion and pollutant formation processes in a 1.9 l IDI diesel engine using SPEED CFD code for a part and full load operations. Hasimoglu [33] has showed that the use of the blends of ethanol and diesel fuels may be an alternative way to reduce both NO_x and soot emissions at the same time without modification of any engine-operating parameters. Hazar [34] has studied the characterization and the effect of using cotton methyl ester as fuel in a LHR diesel engine an alternative way to reduce both these emissions at the same time without modification of any engine-operating parameters.

As can be seen in the relevant literature, there is no more attempt up to now about the 3-D modeling of the combustion process and emissions formation in LHR IDI diesel engines. At present work, this concept is created based on the approach of insulating of piston and liner of chamber. A CFD code has been used to predict combustion process and emissions formation in an LHR IDI engine at various loads and in maximum torque engine speed (730 rpm). This work also demonstrates the usefulness of multi-dimensional modeling for complex geometries, such as in LHR IDI diesel engines, to gain more insight into the flow field, combustion process and emission formation.

Initial and boundary condition

Numerical calculations are conducted at closed system from Intake Valve Closure (IVC) at 165° CA bTDC to Exhaust Valve Open (EVO) at 180° CA aTDC. The numerical grid for modeling of geometry engine includes a maximum of 42200 cells at 165° CA bTDC and generated by automated mesh generation of AVL FIRE soft ware. The present resolution was found to give adequately grid independent results. Injector has single hole and mounted in pre-chamber as shown in fig. 1. Initial pressure in the cylinder is set to 86 kPa and initial temperature is designed to be 384 K. These values for pressure in-cylinder was chosen according to experimental data and for temperature in-cylinder is calculated by air-fuel ratio. All boundaries temperatures were assumed to be constant throughout the simulation, but allowed to vary at various combustion chamber surfaces. Boundary temperatures for two cases in the combustion chamber are: head temperature: 550 K, piston temperature: 590 K, and cylinder temperature: 450 K, present work is studied at full load mode and the engine speed is 730 rpm. All boundary temperatures were assumed to be constant throughout the simulation, but allowed to vary with the combustion chamber surface regions.

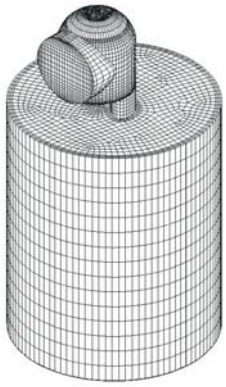

Figure 1(a). Mesh of the Lister 8.1 indirect injection diesel engine

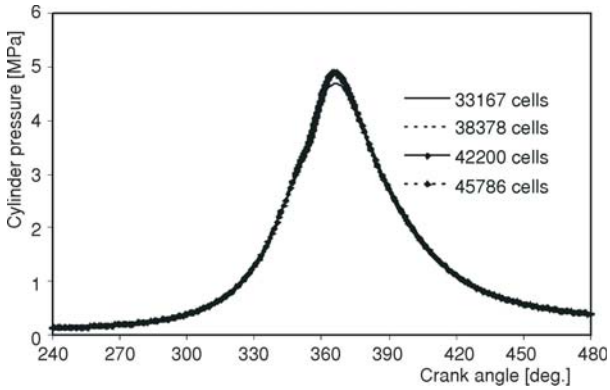

Figure 1(b). Grid dependency based on the in-cylinder pressure

Model formulation

The numerical modeling with above boundary conditions is carried out for Lister 8.1 indirect injection diesel engine with the specification on tab. 1. The governing equations include species, momentum, and energy with appropriate turbulent model (RNG k-ε) [35] and solved from IVC to EVO. Standard WAVE break-up model [36] is used in order to simulating of the primary and secondary atomization of the spray and resulting droplets. Also drop parcels are injected in cylinder with diameters equal to the nozzle exit diameter. The Dukowicz [37] model is used for modeling of the heat up and evaporation of the droplets. A Stochastic dispersion model is employed to take the effect of interaction between the particles and the turbulent eddies into account by adding a fluctuating velocity to the mean gas velocity [38]. This model assumes that the fluctuating velocity has a randomly Gaussian distribution. The interaction of spray and wall is simulated based on the spray/wall impingement model of [39]. Modeling of the auto ignition is based on Shell auto-ignition [40]. This generic mechanism includes 6 species as hydrocarbon fuel, oxidizer, total radical pool, branching agent, intermediate species and products. Also, the

Table 1. Specifications of Lister 8.1 IDI diesel engine

Cycle type	Four stroke
Number of cylinders	1
Injection type	IDI
Cylinder bore × stroke	0.1141 mm × 0.1397 mm
L/R	4
Displacement volume	1.43e–3 m^3
Compression ratio	17.5 : 1
$V_{pre\text{-}chamber}/V_{TDC}$	0.7
Full load injected mass	6.4336e–5 kg per cycle
Part load injected mass	3.2009e–5 kg per cycle
Injection pressure	88.8 bar
Power at 850 rpm	5.9 kW
Power at 650 rpm	4.4 kW
Start injection timing	20° bTDC
Nuzzle diameter at hole center	0.003 m
Number of nuzzle holes	1
Nozzle outer diameter	0.0003 m
Spray cone angle	10°
Valve timing	IVO = 5° bTDC
	IVC = 15° aBDC
	EVO = 55° bBDC
	EVC = 15° aTDC

important stages of auto ignition such as initiation, propagation, branching and termination were presented by generalized reactions [38, 40]. The Eddy Break-up model (EBU), which is based on turbulent mixing, is used for modeling of the combustion process [38] as follows:

$$\overline{\rho \dot{r}_{fu}} = \frac{C_{fu}}{\tau_R}\bar{\rho}\min\left(\bar{y}_{fu}, \frac{\bar{y}_{ox}}{S}, \frac{C_{pr}\bar{y}_{pr}}{1+S}\right) \quad (1)$$

where it is assumed in this model that in premixed turbulent flames, the reactants are contained in the same eddies and are separated from eddies containing hot combustion products. The rate of dissipation of these eddies determines the rate of combustion. Because chemical reaction occurs fast, it is assumed that the combustion is mixing controlled. The first two terms in the "minimum value of" operator determine whether fuel or oxygen is present in limiting quantity, and the third term is a reaction probability which ensures that the flame is not spread in the absence of hot products. Equation (1) also includes two constant coefficients (C_{fu}, C_{pr}) and τ_R is the turbulent mixing time scale for chemical reaction.

NO_x formation is modeled by the Zeldovich mechanism and soot formation is modeled by Kennedy, Hiroyasu, and Magnussen mechanism [41]. The governing equations for unsteady, compressible, turbulent reacting multi-component gas mixtures flow and thermal fields were solved from IVC to EVO by the commercial AVL-FIRE CFD code [38].

Results and discussion

The calculations are carried out for the single cylinder Lister 8.1 IDI diesel engine and the operating conditions are 25%, 50%, 75%, and 100% loads at maximum torque engine speed 730 rpm.

Fiures 2(a), 2(b), and 2(c) show the comparison of computed and measured mean in-cylinder pressure, soot, and NO_x emissions in baseline engine at full load operation, respectively. These experimental tests were carried out for baseline engine as Ph. D. thesis at Tabriz University [42]. They show that both computational and experimental data for cylinder pressure and emissions are in good agreement. The peak pressures discrepancy between experiment and numerical values are less than 0.2%. The peak of cylinder pressure is 50.2 bar, which occurs at 366° CA (4° CA after TDC). The start of injection and combustion are at 348 and 351° CA for computed and measured results, respectively; in other words, the ignition delay dwell is 3° CA. It means that the ignition delay is quite close to the chemical ignition delay and that the physical

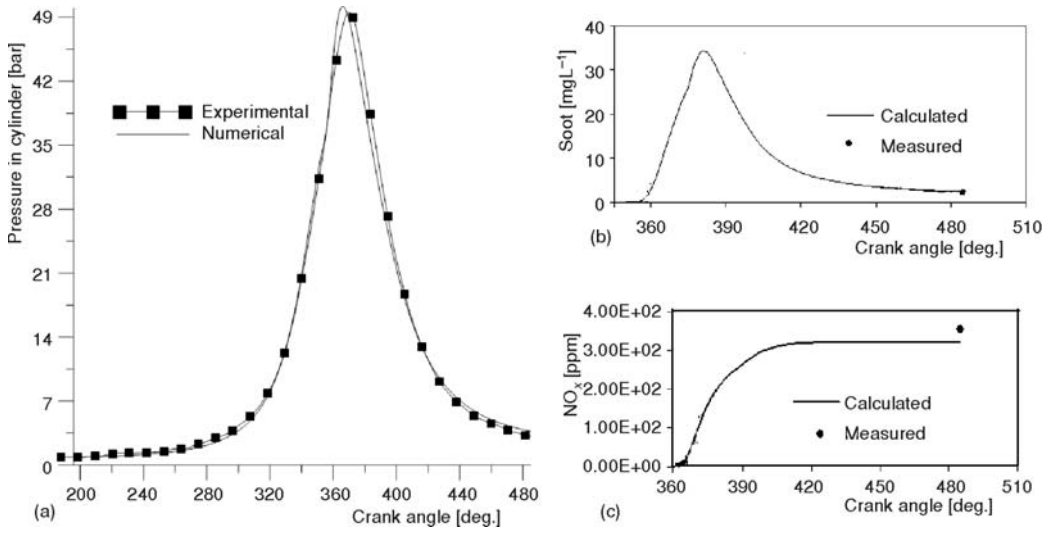

Figure 2. Comparison of measured [42] and calculated pressure and emissions at full load operation

ignition delay is very short, because of higher turbulence intensity and rapid evaporation of the small droplets injected through the small injector gap at the start of injection. Figure 2(b) indicate that the predicted total in-cylinder NO_x emission for baseline, agrees well with the engine-out measurements [42]. Heywood [4] explains that the critical time for the formation of oxides of nitrogen in compression ignition engines is between the start of combustion and the occurrence of peak cylinder pressure when the burned gas temperatures are the highest. The trend of calculated NO_x formation in the chamber agrees well with the Heywood's explanations. As temperature cools due to volume expansion and mixing of hot gases with cooler burned gas, the equilibrium reactions are quenched in the swirl chamber and main chamber. As can be seen

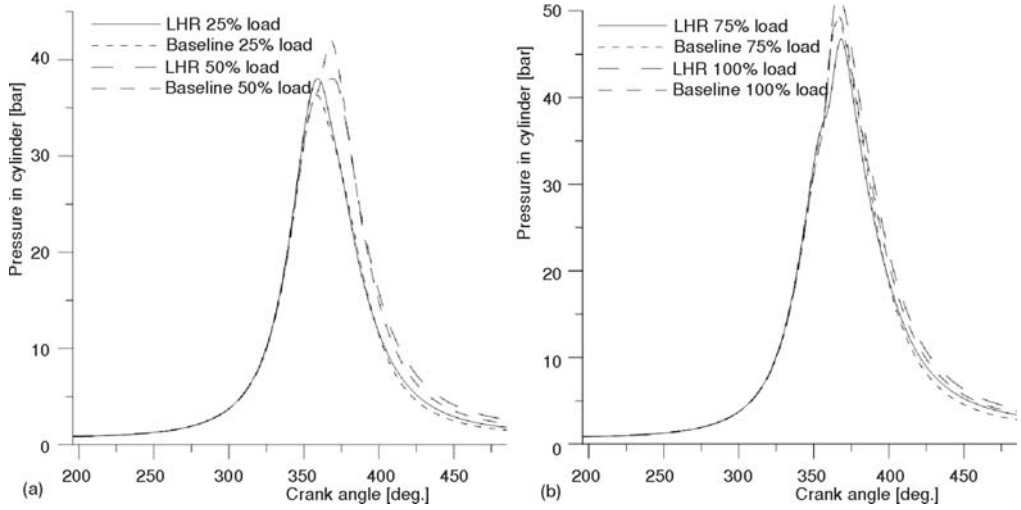

Figure 3. The variation of pressure in cylinder with crank angle position for various loads at two LHR and baseline engine cases

from the fig. 1(c), the predicted total in-cylinder soot emission for the baseline case, as well as calculated NO_x, agrees well with the engine-out measurements [42]. Such verification between the experimental and computed results gives confidence in the model prediction and suggests that the model may be used at future works.

Figures 4(a) and 4(b) show the variation of temperature in cylinder with crank angle position for various loads at two LHR and baseline engine cases. It is clear from these figures that the temperature in cylinder increases at compression stroke due to work transfer for two cases and this increase is more for LHR engine due to insulation of some parts of combustion chamber. At time of start injection the difference of temperature in cylinder for LHR engine and baseline are 33, 33.3, 76, and 73.2 for 25%, 50%, 75%, and 100% loads, respectively. Similar ignition delays and fast increasing of temperature can be observed after start of combustions at

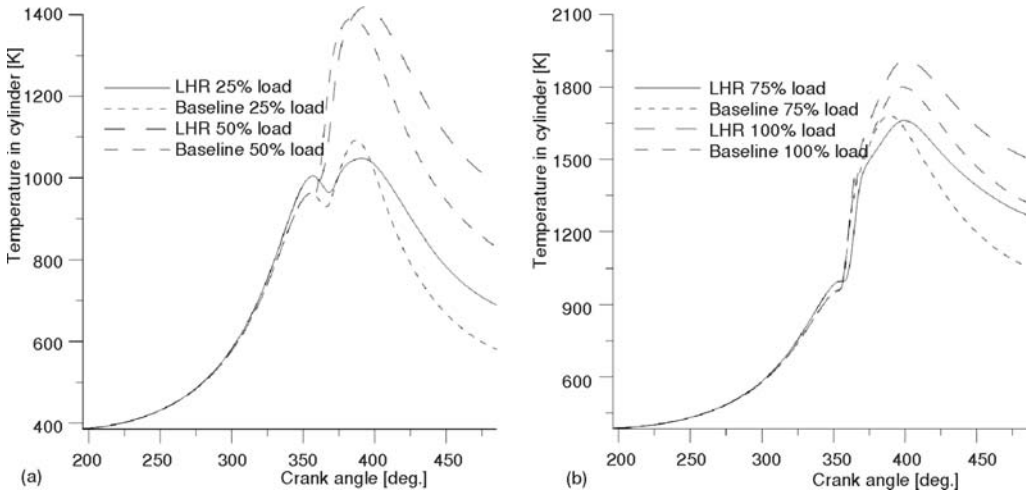

Figure 4. The variation of temperature in cylinder with crank angle position for various loads at two LHR and baseline engine cases

LHR engine for two cases at 25% and 100% load. At 50% and 75% load operations, ignition delay periods of LHR engine case are longer than those of baseline case. After end of combustion period and in exhaust valve opening time, the temperature in cylinder increases considerably at LHR cases because of longer combustion duration. Figures 5(a) and 5(b) show the variations of heat loss to cylinder walls with crank angle position for various loads at two LHR and baseline engine. As shown in these figures that heat loss in LHR case is lower than baseline at compression stroke. The comparison of the results for two cases show that when the load increases from 25% to 100% in 25% steps, heat loss in LHR engine decrease 40.3%, 44.7%, 44.6%, and 45.2%, respectively. Figures 6(a) and 6(b) show the variation of heat release rate with crank angle position for various loads at two cases. As shown in these figures that the start of combustions is the same for 25% and 100% load, while start of combustion is earlier for baseline engine at 50% and 75% loads. Also, combustion duration increases at LHR cases except for 100% load. In 100% load operation, combustion duration is the same for two cases because of similar ignition delays and more fuel injection in two cases. The rate of heat release at premixed phase is lower in LHR case than that of baseline engine. Higher temperature in cylinder at before of fuel injection and more fuel wall impingement may be as the main reasons for this reduction.

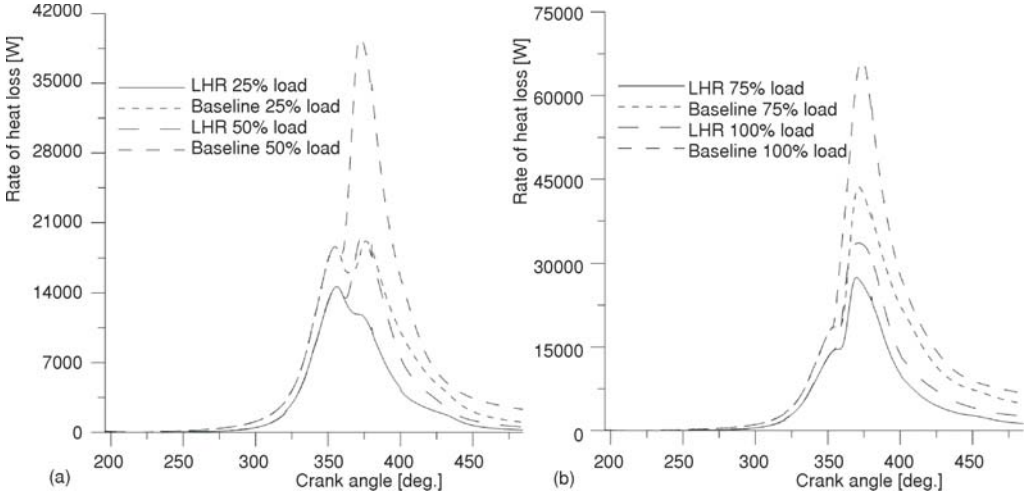

Figure 5. The variation of heat loss with crank angle position for various loads at two LHR and baseline engine cases

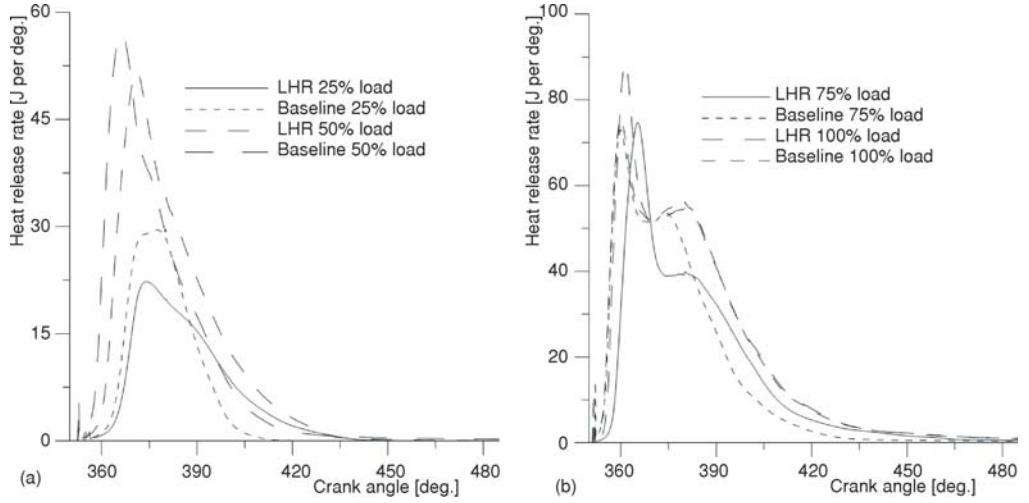

Figure 6. The variation of heat release rate with crank angle position for various loads at two LHR and baseline engine cases

Figures 7(a) and 7(b) show the variation of accumulative heat release with crank angle position for various loads at two cases. Also, as shown in these figures that the start of combustion is the same for 25% and 100% load, while start of combustion is earlier for baseline engine at 50% and 75% loads. The accumulative heat release rates are the same for two cases at various loads due to similar mass fuel injections. Figures 8(a) and 8(b) show the variation of NO_x emission amount with crank angle position for various loads at two cases. Altogether, as has been shown that, except for the full load operation, NO_x emission amount increases in LHR engine in comparison to baseline. At full load operation, the amount of NO_x emission decreases 13.5% at LHR engine compared to baseline engine. The main reason for this decreasing is may be the slight retarding of combustion process in LHR case, as shown in fig. 6(b). This result shows that

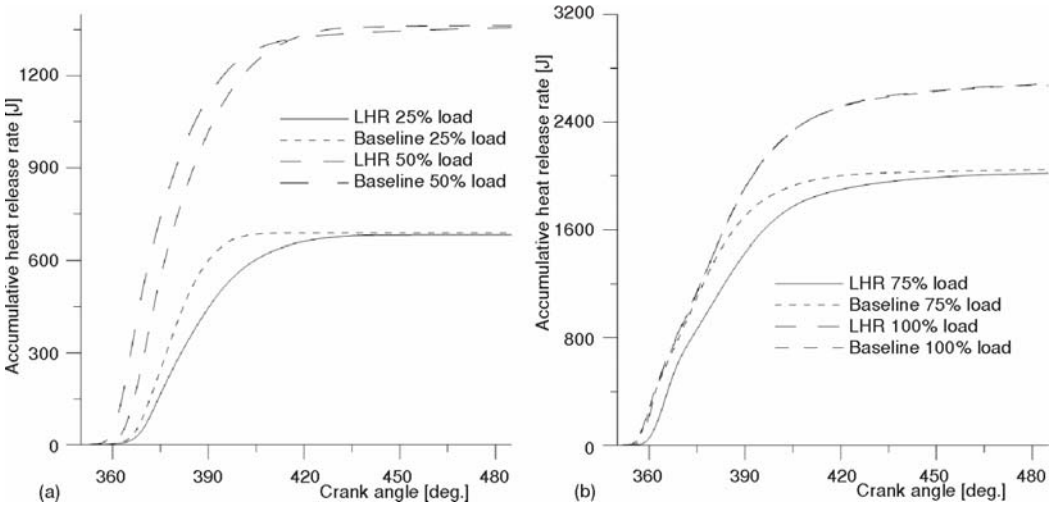

Figure 7. The variation of accumulative heat release with crank angle position for various loads at two LHR and baseline engine cases

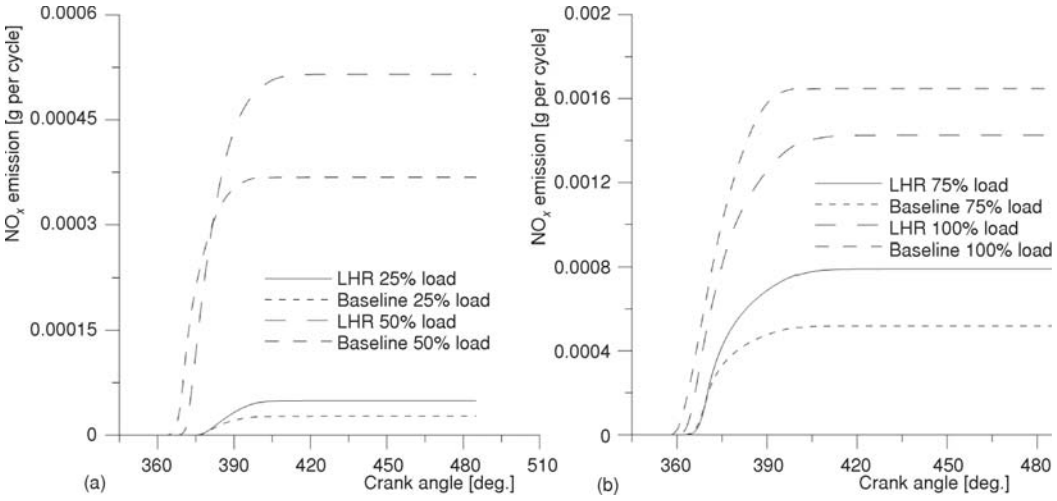

Figure 8. The variation of NO_x mass per cycle with crank angle position for various loads at two LHR and baseline engine cases

at full load, the effect of combustion timing is more considerable than the peak temperature in cylinder.

Figures 9(a) and 9(b) show the variation of soot emission amount with crank angle position for various loads at two cases. These figures show the overall soot concentration inside a combustion chamber as a function of crank angle. Soot emission amount decreases in LHR engine considerably in comparison to baseline. At full load operation, the amount of soot emission decreases 54.5% at LHR engine compared to baseline engine. The main reason for this decreasing is may be the more soot oxidation at higher temperature in power stroke in comparison to baseline. Most of the large amount of soot produced at early crank angles is consumed again at

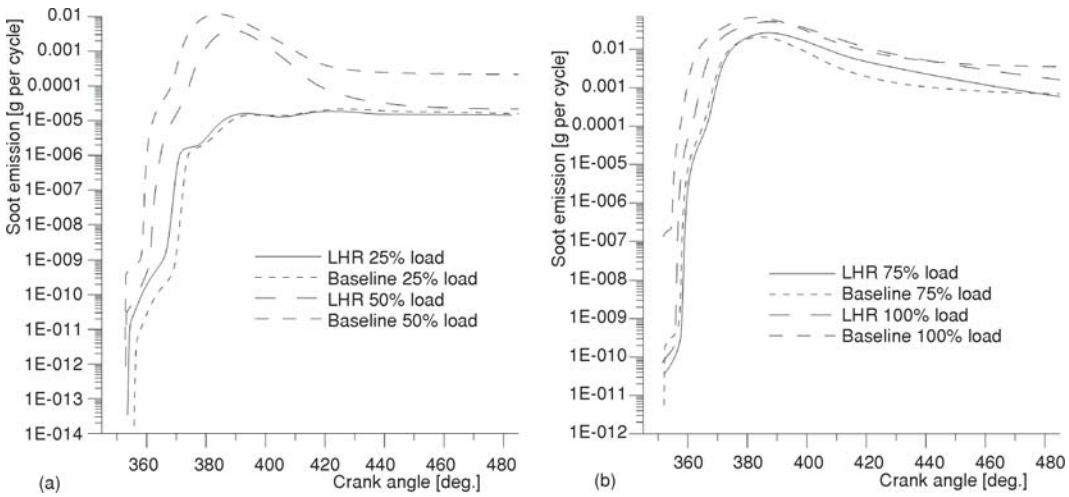

Figure 9. The variation of soot mass per cycle with crank angle position for various loads at two LHR and baseline engine cases

later crank angles especially at higher temperature in cylinder at power stroke, and the remaining mass of soot, which is finally detected in the exhaust gases, is only a very small fraction of the initial one. Figures 10(a), 10(b) and 10(c) represent the evolution of temperature, NO_x and soot emissions at 360°, 380°, 400°, and 420° crank angles for two cases at full load operating conditions.

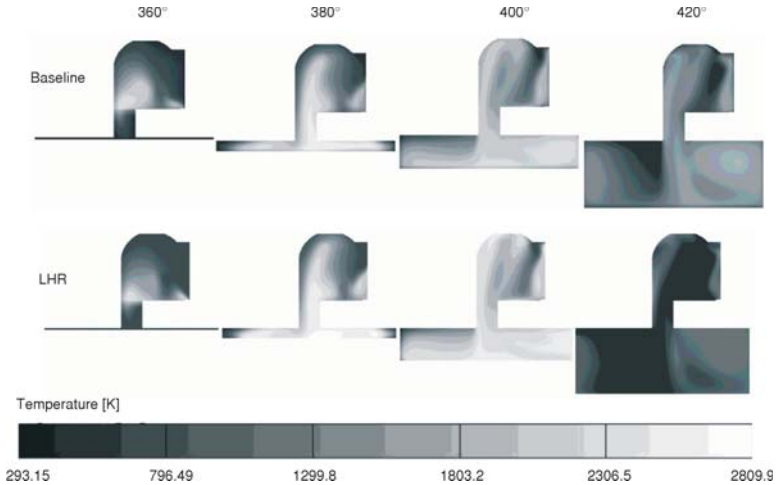

Figure 10(a). Temperature contour plots at two cases for full load operation at 360°, 380°, 400°, and 420° CA

It is clear from fig. 10(a) that, at 360° CA , flame propagations (temperature contours) are similar for two cases and combustion started at the upper edge of swirl chamber throat (stoichiometric zone) and then propagated to pre and main chamber at 380° CA . Also the development of the temperature fields at two cases between 360 and 380° CA show that the axial and

the radial penetrations of the flame front are almost equal. Thus, the flame front reaches the lateral cylinder wall and the cylinder wall opposite to the pre-chamber at approx. the same time. It reveals that the flame started in pre-chamber and then invades a large portion of the main-chamber very quickly. Flame distribution which is shown in this figure also indicates that the swirl generated in swirl chamber during the compression stroke becomes gradually weaker due to opposing flow in glow plug channel (do not shown contours). Therefore, at the end of injection period at 380° CA the flame reaches to near injector location without distortion. Also the similar trends are observed for flame temperature distribution at 360° CA and 380° CA. This would result in similar the mixture formation processes for two cases at these crank angles. In the front view at 400° CA, the hot gas from the pre-chamber reaches the opposite side of main chamber. This leads to the formation of two large eddies each occupying a half of the main chamber and staying centered with respect to the two half of the bowl(don't shown contours). After 400° CA, these regions transfer in the main combustion chamber and therefore, at 50% load operation most of NO_x emission engine form in the main chamber or transfer to in it from pre-chamber.

At figs. 10(b) and 10(c), the production of NO_x and soot in the main and pre-chamber are discussed for two cases at full load operation. It can be seen from fig. 10(b) that at 380° CA the NO_x is produced in the throat and main chamber for two cases. At 400° CA and 420° CA reducing NO_x quantities in the swirl chamber throat is due convection to the main chamber.

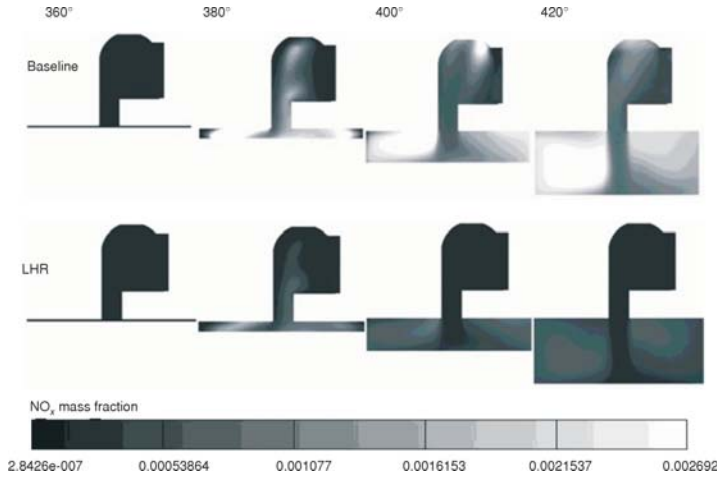

Figure 10(b). Contour plots of NO_x mass fraction at two cases for full load operation at 360°, 380°, 400°, and 420° CA

Finally in figs. 10(c), we present the evolution of the soot mass in the main and pre chambers for two cases full load operations, respectively. As indicated by these figures, in the two cases at full load conditions, the main cause of the exhaust smoke is spray-wall impingement which leads to fuel adhesion on the wall and the stagnation of a rich fuel-air mixture. At 420° CA, dense soot in the main chamber disappears because of complete oxidation. The adherent fuel is not quickly evaporated and formed fuel vapor is hardly carried out of this area, because the stagnation zone is formed here due to the chamber shape. Thus, the rich fuel-air mixture stagnates in this zone under the condition of high temperature and insufficient oxygen to form the dense soot cloud. At 360° CA, the soot is produced in regions of high fuel concentrations, when cold fuel is injected into areas of hot gases at upper edge of swirl chamber throat.

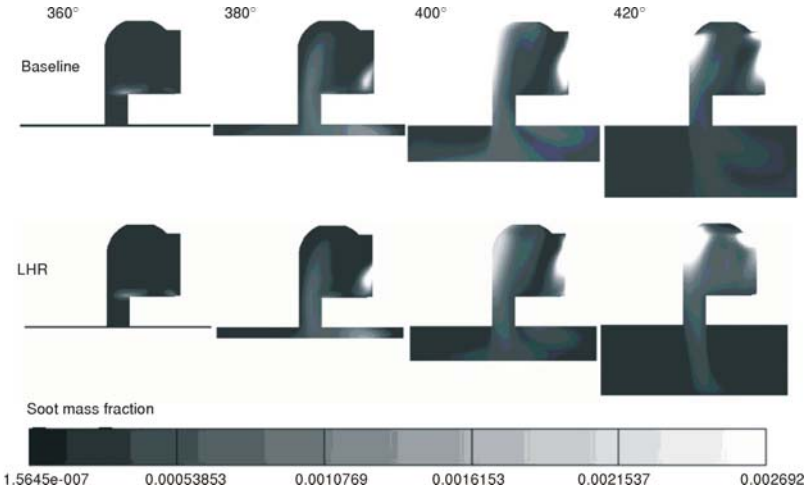

Figure 10(c). Contour plots of soot mass fraction at two cases for full load operation at 360°, 380°, 400°, and 420° CA

Conclusions

At the present work, combustion processes and emissions formation of an IDI diesel engine have been studied by a 3-D CFD code at LHR and baseline engine cases. The results for calculated pressure and emissions at full load operation are compared with the corresponding experimental data and show good agreement. Such verification between the experimental and computed results gives confidence in the model prediction at other loads. The results of the study, when the load increases from 25% to 100% in 25% steps, are as follows.

- Heat loss from cylinder walls at LHR engine decrease 40.3%, 44.7%, 44.6%, and 45.2% in comparison to baseline engines.
- NO_x mass per cycle in LHR engine at 25%, 50%, and 75% load increases 82%, 40%, and 52% respectively, while this value decreases 13.5% at full load operation.
- Soot mass per cycle in LHR engine decreases 91%, 90%, 14.7%, and 54.4%, respectively, in comparison to baseline engine.
- Engine efficiency at LHR engine increases 39.2%, 13.7%, 13.9%, and 6.3% in comparison to baseline engines.

The results show that emissions and engine efficiency simultaneously can be improved at full load operation in baseline engine by LHR concept. This result confirmed by experimental investigation of Assanis *et al.* [25]. They have performed experimental investigations in LHR engine and have shown that efficiency increases 10%, exhaust CO levels were lower between 30% and 60% than baseline levels and unburned HC levels were lower 35% to 40% for the insulated pistons. Also, the NO_x concentrations were also 10% to 30% lower due to the changed nature of combustion in the insulated engines. Finally, smoke emissions decreased slightly in the insulated engines.

References

[1] Canakci, M., Combustion Characteristics of a Turbocharged DI Compression Ignition Engine Fueled with Petroleum Diesel Fuels and Biodiesel, *Bioresource Technology, 98* (2007), 6, pp. 1167-1175
[2] Ozsezen, A. N., *et al*., Effects of Biodiesel from Used Frying Palm Oil on the Performance, Injection, and Combustion Characteristics of an Indirect Injection Diesel Engine, *Energy and Fuels, 22* (2008), 2, pp. 1297-1305

[3] Ghojel, J., Honnery, D., Heat Release Model for the Combustion of Diesel Oil Emulsions in DI Diesel Engines, *Appl. Therm. Eng., 25* (2005), 14-15, pp. 2072-2085
[4] Heywood, J. B., *Internal Combustion Engine Fundamentals*, McGraw Hill International Editions, New York, USA, 1988, pp. 491-497
[5] ***, Bosch Handbook, Diesel-Engine Management: An Overview; Robert Bosch GmbH: Stuttgart, Germany, 2003, pp. 24-27
[6] Owen, K., Coley, T., *Automotive Fuels Reference Book*, 2nd ed., SAE, Warrendale, Penn., USA, 1995, p. 375
[7] Abdel-Rahman, A. A., A Review: On the Emissions from Internal-Combustion Engines, *Int. J. Energy Res., 22* (1998), 6, pp. 483-513
[8] Iwazaki, K., *et al.*, Improvement of Fuel Economy of an Indirect Injection (IDI) Diesel Engine with Two-Stage Injection, *Energy, 30* (2005), 2-4, pp. 447-459
[9] Rakopoulos, C. D., *et al.*, Study of Combustion in a Divided Chamber Turbocharged Diesel Engine by Experimental Heat Release Analysis in its Chambers, *Appl. Therm. Eng., 26* (2006), 14-15, pp. 1611-1620
[10] Kamo, R., Bryzik, W., Cummins Adiabatic Engine Program, SAE paper 83314, 1983
[11] Kamo, R., *et al*., Thermal Barrier Coating for Diesel Engine Piston, ASME Transactions, Paper 80-DGP-14, 1980
[12] Thring, R. H., Low Heat Rejection Engines, SAE paper 860314, 1986
[13] Parlak, A., *et al*., Performance and Exhaust Emission Characteristics of a Lower Compression Ratio LHR Diesel Engine, *Energy Conversion & Management, 44* (2003), 1, pp. 163-175
[14] Parlak, A., *et al*., Performance Optimization of an Irreversible Dual Cycle with Respect to Pressure Ratio and Temperature Ratio – An Experimental Results of a Ceramic Coated IDI Diesel Engine, *Energy Conversion & Management, 45* (2004), 7-8, pp. 1219-1232
[15] Kamo, R., Bryzik, W., Adiabatic Turbo Compound Engine Program, SAE paper 810070, 1981
[16] Wallace, F. J., *et al*., Effect of Partial Suppression of Heat Loss of Coolant on the High Output Diesel Engine Cycle. SAE paper 790823, 1979
[17] Parker, D.A., Donison, G., The Development of an Air Gap Insulated Piston, SAE paper 870652, 1985
[18] Kamo, R., *et al.*, Injection Characteristics that Improve Performance of Ceramics Coated Diesel Engines, SAE technical paper 1999-01-0972, 1999
[19] Parlak, A., *et al*., The Effects of Injection Timing on NO_x Emissions of a Low Heat Rejection Indirect Diesel Injection Engine, *Applied Thermal Engineering, 25* (2005), 17-18, pp. 3042-3052
[20] Buyukkaya, E., Cerit, M., Experimental Study of NO_x Emissions and Injection Timing of a Low Heat Rejection Diesel Engine, *International Journal of Thermal Sciences, 47* (2008), 8, pp. 1096-1106
[21] Dickey, D. W., The Effect of Insulated Chamber Surfaces on Direct Injected Diesel Engine Performance, Emissions, and Combustion, SAE paper 890292, 1989
[22] Jaichandar, S., Tamilporai, P., The Status of Experimental Investigations on Low Heat Rejection Engines, SAE technical paper 2004-01-1453, 2004
[23] Amann, C. A., Promises and Challenges of the Low-Heat-Rejection Diesel, *Journal of Engineering for Gas Turbines and Power, 110* (1988), pp. 475-481
[24] Wang, Y., *et al*., An Observation of High Temperature Combustion Phenomenon in Low-Heat- Rejection Diesel Engines, SAE paper 940949, 1994
[25] Assanis, D., *et al*., The Effects of Ceramic Coatings on Diesel Engine Performance and Exhaust Emissions, SAE paper 910460, 1991
[26] Taymaz, I., An Experimental Study of Energy Balance in Low Heat Rejection Diesel Engine, *Energy, 31* (2006), 2-3, pp. 364-371
[27] Parlak, A., The Effect of Heat Transfer on Performance of the Diesel Cycle and Exergy of the Exhaust Gas Stream in a LHR Diesel Engine at the Optimum Injection Timing, *Energy Conversion and Management, 46* (2005), 2, pp. 167-179
[28] Hejwowski, T, Weronski, A., The Effect of Thermal Barrier Coatings on Diesel Engine Performance, *Vacuum, 65* (2002), p. 427
[29] Toyama, K., *et al*., Heat Insulated Turbocompound Engine, SAE paper 831345, 1983
[30] Pinchon, P., Three Dimensional Modeling of Combustion in a Pre-Chamber Diesel Engine, SAE paper 890666, 1989
[31] Zellat, M., *et al*., Three Dimensional Modeling of Combustion and Soot Formation in an Indirect Injection Diesel Engine, SAE paper 900254, 1990

[32] Strauss, T. S., Schweimer, G. W., Combustion in a Swirl Chamber Diesel Engine Simulation by Computation of Fluid Dynamics, SAE paper 950280, 1995
[33] Hasimoglu, C., Exhaust Emission Characteristics of a Low-Heat-Rejection Diesel Engine Fuelled with 10 Per Cent Ethanol and 90 Per Cent Diesel Fuel Mixture, *Proceedings*, Institution of Mechanical Engineers, Part D: *Journal of Automobile Engineering, 1* (2008), 222, pp. 93-100
[34] Hazar, H., Characterization and Effect of Using Cotton Methyl Ester as Fuel in a LHR Diesel Engine, *Energy Conversion and Management, 52* (2011), 1, pp. 258-263
[35] Han, Z., Reitz, R. D., Turbulence Modeling of Internal Combustion Engines Using RNG Models, *Combustion Science and Technology, 106* (1995), pp. 267-295
[36] Liu, A. B., Reitz, R. D., Modeling the Effects of Drop Drag and Break-Up on Fuel Sprays, SAE paper 930072, 1993
[37] Dukowicz, J. K., Quasi-Steady Droplet Change in the Presence of Convection, Informal Report Los Alamos Scientific Laboratory, LA7997-MS, Los Alamos, N. Mex., USA
[38] ***, *AVL FIRE user manual* V. 8.5; 2006
[39] Naber, J. D., Reitz, R. D., Modeling Engine Spray/Wall Impingement, SAE paper 880107, 1988
[40] Halstead, M., *et al*., The Auto Ignition of Hydrocarbon Fueled at High Temperatures and Pressures – Fitting of a Mathematical Model, *Combustion Flame, 30* (1977), pp. 45-60
[41] Patterson, M. A., *et al*., Modeling the Effects of Fuel Injection Characteristics on Diesel Engine Soot and NOx Emissions, SAE paper 940523, 1994
[42] Mohammahi Kusha A., *et al*., Ignition of Dual Fuel Engines by Using Free Radicals Existing in EGR Gases, Ph. D. thesis, Faculty of Mechanical Engineering, Tabriz University, Iran, 2008

Paper submitted: February 3, 2013
Paper revised: August 12, 2013
Paper accepted: August 26, 2013